Available online at www.sciencedirect.com
SCIENCE DIRECT®
Journal of Computational Physics 206 (2005) 150–161
JOURNAL OF COMPUTATIONAL PHYSICS
www.elsevier.com/locate/jcp

A 2D lattice Boltzmann study on electrohydrodynamic drop deformation with the leaky dielectric theory

Junfeng Zhang, Daniel Y. Kwok *

Nanoscale Technology and Engineering Laboratory, Department of Mechanical Engineering, University of Alberta, Edmonton, Alta., Canada T6G 2G8

Received 21 April 2004; received in revised form 23 November 2004; accepted 25 November 2004
Available online 25 January 2005

Abstract

The lattice Boltzmann method (LBM) and electrohydrodynamics are both active subjects in fluid mechanics research in recent years. In this paper, we present a method to apply a multicomponent LBM to electrohydrodynamics studies. A series of drop deformation simulations under the influence of an electric field were carried out and the results are in good agreement with other theoretical and experimental studies. Given that no special treatment of fluid–fluid interfaces is required for multiphase/multicomponent LBM, our method could be an excellent alternative to electrohydrodynamics studies than traditional computational fluid dynamics methods. Further, our algorithm and simulation can be readily implemented to the more complex electrohydrodynamic systems. To our knowledge, this represents the first LBM study on electrohydrodynamics.

Keywords: Lattice Boltzmann method; Electrohydrodynamics; Leaky dielectric theory; Multicomponent flow; Drop deformation; Diffuse interface

1. Introduction

Electrohydrodynamics (EHD) is the study of fluid motions induced by an applied electric field [1,2]. The earliest EHD observation can be traced back to the seventeenth century, in which Gilbert showed that a spherical water drop sitting on a dry surface deformed into a cone when a piece of rubbed amber was brought above at a given distance [3]. Modern industrial and scientific applications of EHD are abundant, including ink jet printing, electrostatic painting, boiling and biotechnology [1,4,5].

* Corresponding author. Tel.: +1 780 492 2791; fax: +1 780 492 2200.
E-mail address: daniel.y.kwok@ualberta.ca (D.Y. Kwok).

0021-9991/$ - see front matter © 2005 Elsevier Inc. All rights reserved.
doi:10.1016/j.jcp.2004.11.032

EHD deformation of fluid–fluid interfaces, especially the deformation of a drop suspending in a second fluid, has been studied extensively [2,5–15]. It was Taylor who firstly introduced the well-known leaky dielectric model [1,2,7]. In this model, fluids are considered to have low conductivities and, when an electric field is applied, free charge can appear only at the fluid–fluid interfacial region. The leaky dielectric model is known to provide accurate qualitative and quantitative results [1,16]. Recently, Trau et al. [13] extended this theory to a diffuse interface and compared its prediction with experiments. Obviously, analytical applications are limited to simple systems and numerical methods such as a finite element method are usually required [13,14,17] for more complex systems.

Recently, the lattice Boltzmann method (LBM) has experienced tremendous development in simulating fluid hydrodynamic behaviors [18,19]. Compared with traditional computational fluid dynamics, LBM algorithms are much easier to be implemented to complex solid or free boundaries even for multiphase/multicomponent fluid systems. The attractiveness of LBM for multiphase/multicomponent studies lies in the fact that, unlike other numerical schemes, no special treatment or attention is required for the fluid–fluid interfaces [20–22]. In this paper, we employ the leaky dielectric theory with diffuse interfaces according to Trau et al. [13] and present an LBM scheme to simulate electrohydrodynamic behaviors. As an example, drop deformation simulations will be conducted and the results will be compared with those from theoretical predictions and experiments. It will be apparent below that the LBM proposed here could be an excellent alternative in future electrohydrodynamics studies.

2. Theory and method

2.1. Interparticle potential LBM model for multicomponent fluid

In this section, a brief review of Shan and Chen's interparticle potential LBM model [20] will be given as this model has been widely employed in different multiphase/multicomponent and interfacial situations [23–28]. Our description will be limited to a D2Q9 (two dimensions, nine lattice velocities) LBM version. In this model, the following lattice Boltzmann equation is solved for a S-component fluid

$$f_i^{(k)}(\mathbf{x}+\mathbf{e}_i, t+1) - f_i^{(k)}(\mathbf{x}, t) = -\frac{f_i^{(k)}(\mathbf{x}, t) - \bar{f}_i^{(k)}(\mathbf{x}, t)}{\tau^{(k)}}, \tag{1}$$

where $f_i^{(k)}(\mathbf{x}, t)$ is the number density distribution of the kth component in the ith lattice velocity direction $\mathbf{e}_i$ at position $\mathbf{x}$ and time t; $\tau^{(k)}$ is the relaxation time of the kth component and $\bar{f}_i^{(k)}(\mathbf{x}, t)$ is the corresponding equilibrium distribution given below [29,30]:

$$\begin{aligned}
\bar{f}_0^{(k)} &= \alpha^{(k)} n^{(k)} - \frac{2}{3} n^{(k)} \bar{\mathbf{u}}^{(k)} \cdot \bar{\mathbf{u}}^{(k)}, \\
\bar{f}_i^{(k)} &= \frac{(1-\alpha^{(k)}) n^{(k)}}{5} + \frac{1}{3} n^{(k)} \mathbf{e}_i \cdot \bar{\mathbf{u}}^{(k)} + \frac{1}{2} n^{(k)} (\mathbf{e}_i \cdot \bar{\mathbf{u}}^{(k)})^2 - \frac{1}{6} n^{(k)} \bar{\mathbf{u}}^{(k)} \cdot \bar{\mathbf{u}}^{(k)}, \quad i = 1\text{–}4, \\
\bar{f}_i^{(k)} &= \frac{(1-\alpha^{(k)}) n^{(k)}}{20} + \frac{1}{12} n^{(k)} \mathbf{e}_i \cdot \bar{\mathbf{u}}^{(k)} + \frac{1}{8} n^{(k)} (\mathbf{e}_i \cdot \bar{\mathbf{u}}^{(k)})^2 - \frac{1}{24} n^{(k)} \bar{\mathbf{u}}^{(k)} \cdot \bar{\mathbf{u}}^{(k)}, \quad i = 5\text{–}8.
\end{aligned} \tag{2}$$

The discrete lattice velocities in the above equations are:

$$\begin{aligned}
\mathbf{e}_0 &= \mathbf{0}, \\
\mathbf{e}_i &= \left(\cos\frac{i-1}{2}\pi, \sin\frac{i-1}{2}\pi \right), \quad i = 1\text{–}4, \\
\mathbf{e}_i &= \sqrt{2}\left(\cos\frac{2i-9}{4}\pi, \sin\frac{2i-9}{4}\pi \right), \quad i = 5\text{–}8.
\end{aligned} \tag{3}$$

In Eq. (2), $\alpha^{(k)}$ is a parameter related to the sound speed $c_s^{(k)}$ in a pure kth component media by $(c_s^{(k)})^2 = 3(1-\alpha^{(k)})/5$ [27]. The total number density of the kth component $n^{(k)}$ is just the sum of $f_i^{(k)}$ as $n^{(k)} = \sum_i f_i^{(k)}$ and its mass density $\rho^{(k)}$ can therefore be easily obtained by multiplying $n^{(k)}$ with the corresponding molecular mass $m^{(k)}$ as $\rho^{(k)} = m^{(k)}n^{(k)}$. The velocity of the kth fluid $\mathbf{u}^{(k)}$ is defined through $\mathbf{u}^{(k)} = \sum_i \mathbf{e}_i f_i^{(k)}/\rho^{(k)}$ and the equilibrium velocity $\bar{\mathbf{u}}^{(k)}$ is given by

$$\rho^{(k)}\bar{\mathbf{u}}^{(k)} = \rho^{(k)}\mathbf{u}' + \tau^{(k)}\mathbf{F}^{(k)}, \tag{4}$$

where $\mathbf{u}'$ is a common velocity where an extra component-specific velocity due to interparticle and external forces $\mathbf{F}^{(k)}$ can be added for each component [24]. In our study, $\mathbf{F}^{(k)}$ includes both the fluid–fluid interaction $\mathbf{F}_{\mathrm{Int}}^{(k)}$ and electric force $\mathbf{F}_{\mathrm{Ele}}^{(k)}$, see below. To conserve momentum at each collision in the absence of $\mathbf{F}^{(k)}$, we express $\mathbf{u}'$ as follows:

$$\mathbf{u}' = \left(\sum_k \frac{\rho^{(k)}\mathbf{u}^{(k)}}{\tau^{(k)}}\right) \Bigg/ \left(\sum_k \frac{\rho^{(k)}}{\tau^{(k)}}\right). \tag{5}$$

Following the common treatment [24,26,27], we model the fluid–fluid interaction $\mathbf{F}_{\mathrm{Int}}^{(k)}$ as

$$\mathbf{F}_{\mathrm{Int}}^{(k)}(\mathbf{x}) = -n^{(k)}(\mathbf{x}) \sum_{\mathbf{x}'} \sum_{\bar{k}} G_{k\bar{k}}(\mathbf{x},\mathbf{x}') n^{(\bar{k})}(\mathbf{x}')(\mathbf{x}' - \mathbf{x}). \tag{6}$$

By considering the interactions between nearest neighbors with the value $g_{k\bar{k}}$ characterizing the interaction strength, we reduce the above Green's function $G_{k\bar{k}}(\mathbf{x},\mathbf{x}')$ to

$$G_{k\bar{k}}(\mathbf{x},\mathbf{x}') = \begin{cases} g_{k\bar{k}}, & |\,\mathbf{x}-\mathbf{x}'\,| = 1, \\ g_{k\bar{k}}/4, & |\,\mathbf{x}-\mathbf{x}'\,| = \sqrt{2}, \\ 0, & \text{otherwise.} \end{cases} \tag{7}$$

The Chapman–Enskog method has been applied to the above equations to obtain the continuity and momentum equations with the fluid velocity $\mathbf{u}$ expressed by [31,32]

$$\rho\mathbf{u} = \sum_k \rho^{(k)}\mathbf{u}^{(k)} + \frac{1}{2}\sum_k \mathbf{F}^{(k)}, \tag{8}$$

where the total fluid mass density is $\rho = \sum_k \rho^{(k)}$ and the fluid kinematic viscosity is $v = (2\sum_k \rho^{(k)}\tau^{(k)}/\rho - 1)/6$.

2.2. Leaky dielectric theory with diffuse interfaces

In general, the leaky dielectric model consists of the Navier–Stokes equations to describe fluid motion and an expression for the conservation of current employing an Ohmic conductivity [1,2]. Electric forces experienced by fluid particles can be expressed as a Maxwell stress tensor or as a body force [33]

$$\mathbf{F}_{\mathrm{Ele}} = -\frac{1}{2}\mathbf{E}\cdot\mathbf{E}\nabla\epsilon + q\mathbf{E}, \tag{9}$$

where $\mathbf{E}$ is the electric field, ϵ is the local fluid permittivity and q is the free charge density given by

$$q = \nabla\cdot(\epsilon\mathbf{E}). \tag{10}$$

The electric field can be written as the gradient of a scalar potential U

$$\mathbf{E} = -\nabla U \tag{11}$$

and the charge conservation is governed by [13]

$$\mathbf{u}\cdot\nabla q = \nabla\cdot[\sigma\nabla U + \eta\nabla q], \tag{12}$$

where σ is the local fluid conductivity and η is the ion diffusivity. As the convective $\mathbf{u}\cdot\nabla q$ and diffusive $\nabla\cdot[\eta\nabla q]$ terms are usually small compared to the conduction term $\nabla\cdot[\sigma\nabla U]$, we have simplified Eq. (12) by solving the electric potential U as [13]

$$\nabla\cdot[\sigma\nabla U] = 0. \tag{13}$$

2.3. Implementing LBM to EHD

As mentioned above, the influence of an applied electric field to fluid motion is caused by the electric forces (Maxwell's stresses) because of non-uniform fluid conductivity, permittivity and/or electric field. A typical density distribution across an interface of a two-component system from the LBM model described above is shown in Fig. 1(a). As is typically performed with a one-fluid approximation in liquid mixture studies [34], we assume the mixture dielectric properties to follow

$$\begin{aligned}\epsilon &= \epsilon^{(1)}\rho^{(1)} + \epsilon^{(2)}\rho^{(2)},\\ \sigma &= \sigma^{(1)}\rho^{(1)} + \sigma^{(2)}\rho^{(2)},\end{aligned} \tag{14}$$

where $\epsilon^{(1)}$, $\epsilon^{(2)}$, $\sigma^{(1)}$ and $\sigma^{(2)}$ are constants that can be adjusted to produce different bulk property values. As an example, the variation of conductivity and permittivity from such a model is also displayed in Fig. 1(b). Clearly, these simple expressions generate smooth increasing/decreasing transitions across an interface from one bulk value to another. In Ref. [13], a similar assumption through a prescribed cosine function was also employed to describe such transition behavior.

In principle, Eq. (13) can be solved by any suitable numerical methods to obtain the electric potential/field distribution. To have our algorithm consistent with the above LBM approach to fluid dynamics, we follow the lattice Boltzmann framework proposed by He and Li [35] to solve the electric potential, although other algorithms [35,36] can be more sophisticated. Thus, a new set of particle distributions h_i is introduced and their evolutions are described as

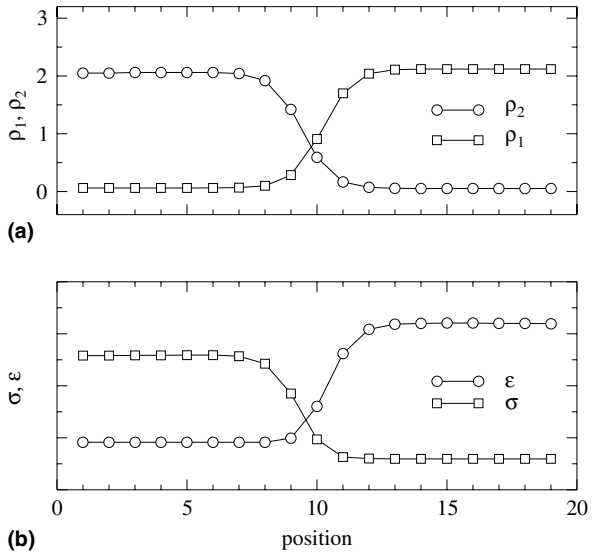

Fig. 1. (a) Typical density distributions across an interface and (b) an example of the conductivity and permittivity from Eq. (14).

$$h_i(\mathbf{x}+\mathbf{e}_i, t+1) - h_i(\mathbf{x}, t) = -\frac{h_i(\mathbf{x}, t) - \bar{h}_i(\mathbf{x}, t)}{\tau^h}, \tag{15}$$

where the equilibrium distributions $\bar{h}_i$ are

$$\begin{aligned} \bar{h}_0 &= \frac{4}{9}U, \\ \bar{h}_i &= \frac{1}{9}U, \quad i = 1\text{–}4, \\ \bar{h}_i &= \frac{1}{36}U, \quad i = 5\text{–}8 \end{aligned} \tag{16}$$

and

$$\tau^h = 3\sigma + 0.5. \tag{17}$$

Through a Chapman–Enskog procedure, Eq. (13) can be recovered with the electric potential U defined as

$$U = \sum_i h_i. \tag{18}$$

As there are two types of fluid particles in this system, the electric force $\mathbf{F}_{\text{Ele}}$ obtained through Eq. (9) has to be separated into two parts and applied onto each kind of particles. Similar to Eq. (14), we divide this force according to the density ratio as:

$$\mathbf{F}_{\text{Ele}}^{(k)} = \frac{\rho^{(k)}}{\rho}\mathbf{F}_{\text{Ele}}. \tag{19}$$

3. Results and discussion

Unless otherwise specified, simulations in this paper were performed over a 128×128 rectangular D2Q9 domain with periodic boundary conditions in both directions for fluid particles. The interaction potential strengths were selected as $g_{11} = g_{22} = 0$ and $g_{12} = g_{21} = 0.1$. The relaxation time for both kinds of fluid particles is $\tau^{(k)} = 1$ with $\alpha^{(k)} = 4/9$. For simplicity, we also set the molecular mass $m^{(k)} = 1$. However, various density and viscosity values can be readily obtained through adjustment of $m^{(k)}$ and $\tau^{(k)}$ [27,37]. When no electric field is applied, the drop formed in the center domain at equilibrium has a radius of 11.22. The boundary conditions for solving the electric potential U are considered not to be affected by the presence of the drop: we maintain constant potential values on the left and right sides of the domain as $U_1 = 127$ and $U_2 = 0$, respectively; along the top and bottom boundary sites, the potential U changes linearly with position. The applied electric field $\mathbf{E}_0$ is thus $E_0 = (U_1 - U_2)/(128 - 1) = 1$ in the horizontal direction, from left to right. As in typical LBM studies, all values given here are dimensionless and can be readily mapped to physical properties [19].

3.1. Evaluation of interfacial tension

Bubble tests were carried out to evaluate the interfacial tension for a given set of simulation parameters. The initial density distribution for component 1 was assigned with a higher density in the center and a lower density elsewhere; the density distribution for component 2 was initially set to be lower in the center and higher elsewhere. After about 10,000 steps, the system reached equilibrium and the drop radius and densities inside and outside were measured. The pressure can be obtained from the densities through the following relation [27]:

$$P = \frac{1}{3}\sum_{k} n^{(k)} + \frac{3}{2}\sum_{k\bar{k}} g_{k,\bar{k}} n^{(k)} n^{(\bar{k})}. \tag{20}$$

According to the Laplace equation of capillary, the pressure difference $P_{\text{in}} - P_{\text{out}}$ across an interface of a 2D drop with a radius r is given by

$$P_{\text{in}} - P_{\text{out}} = \gamma / r, \tag{21}$$

where γ is the interfacial tension. Hereafter, the subscripts 'in' and 'out' specify the fluid phases inside or outside the drop, respectively. Simulation results were plotted in Fig. 2(a) together with a fitted line according to the Laplace equation (21). Clearly, the symbols from our LBM results follow Eq. (21) very well and, from the slope of the fitted line, the interfacial tension γ was found to be 0.181 ± 0.002.

By adjusting the interaction strength g_{12}, different interfacial tension values can be obtained. Fig. 2(b) displays our simulation results for the dependence of interfacial tension γ with the interaction strength g_{12}. Obviously, γ increases with the interaction strength g_{12}, following a linear relationship approximately. Similar dependence behavior was also observed by Yang et al. [38] in studying the bubble growth and detachment using Shan–Chen's multiphase LBM model.

3.2. Drop deformations

As an example to demonstrate the method described above, we study here the deformation behaviors of a 2D drop being suspended in another fluid. For the present LBM approach, drop deformations can be easily produced with different combinations of parameters $\epsilon^{(1)}$, $\epsilon^{(2)}$, $\sigma^{(1)}$ and $\sigma^{(2)}$. The theoretical analysis given by Feng [39] shows that drop deformation D in response to an electric field is [39]

$$D = \frac{d\epsilon_{\text{in}} E_0^2 r_0}{3S(1+R)^2\gamma}, \tag{22}$$

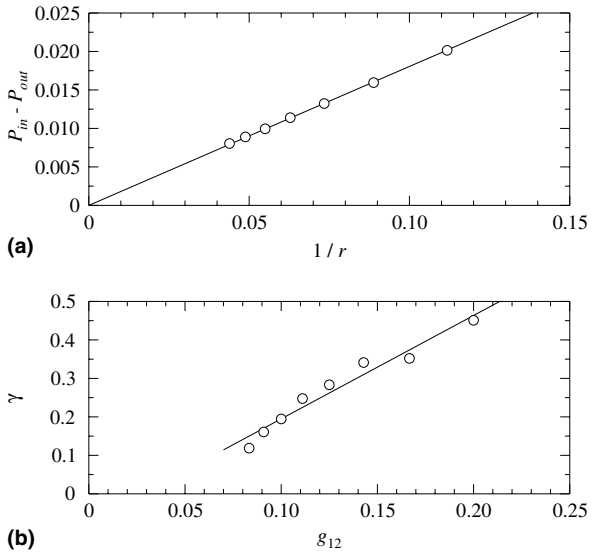

Fig. 2. (a) Evaluation of the interfacial tension γ through the Laplace equation of capillary Eq. (21) and (b) variation of the simulated interfacial tension γ with interaction strength g_{12}.

where $R = \sigma_{in}/\sigma_{out}$ and $S = \epsilon_{in}/\epsilon_{out}$, and r_0 is the initial drop radius before deformation. It should be pointed out that this relation is analogous to that of Taylor's analysis for 3D drops [7]. D is defined by taking the difference between the drop's parallel and transverse axes and divided by their sum [7,39]. d is a discriminating function expressed as [40,39]

$$d = R^2 + R + 1 - 3S. \tag{23}$$

If $d > 0$, the drop will deform into a prolate shape with its longer axis along the electric field direction; and, if $d < 0$, an oblate shape with its shorter axis along the field will result. Although the above equations were derived for a sharp interface, this discriminating function has been found to agree well with the results from experiments and other numerical studies [13]. Our LBM simulations also reconfirm this finding and the results are displayed in Table 1. For all nine cases with different conductivity and permittivity ratios, we found that the deformation D from our LBM simulations (column 6, Table 1) always has the same sign as that of the discriminating function d, confirming the validity of d in predicting such drop deformation behaviors. The deformation values from our simulations (column 6, Table 1) are also in good agreement with the theoretical prediction (column 7, Table 1) when deformation is small. For large deformations, our LBM results are generally larger than those predicted by Eq. (22). Such deviation is not surprising as Eq. (22) was derived based on an assumption of small deformation. For larger drop deformations, Eq. (22) typically under-estimates such deformations, as demonstrated through several other numerical and experimental studies [8,10,41,42].

Fig. 3 displays the results of D as E_0, ϵ_{in}, r_0 and γ are varied independently. In order to maintain constant conductivity R and permittivity S ratios for the simulations in Fig. 3(d), one cannot simply fixed the parameters $\epsilon^{(1)}$, $\epsilon^{(2)}$, $\sigma^{(1)}$ and $\sigma^{(2)}$ as those in Fig. 3(a)–(c); this is due to the variation of fluid density with interaction strength g_{12} and hence the conductivity and permittivity through relation equation (14). Instead, we adjusted these parameters $\epsilon^{(1)}$, $\epsilon^{(2)}$, $\sigma^{(1)}$ and $\sigma^{(2)}$ to produce the specific conductivity and permittivity values inside and outside the drop. The straight lines are the theoretical prediction from Eq. (22). It can be seen in Fig. 3 that, for small deformations ($D \leqslant 0.1$), the simulation results are in good agreement with the those from theory; however, for larger deformation ($D > 0.1$), the calculated values deviate slightly from those of the theory. This finding is again not surprising as Eq. (22) is only expected to be valid with small deformations; and the observed deformation is typically larger than the theoretical prediction for large deformations [8,10,42].

Table 1
Comparison of the discriminating function d with the deformations D from LBM (this work) and theory (Eq. (22)) with different combinations of conductivity and permittivity

$\epsilon^{(1)}$	$\epsilon^{(2)}$	$\sigma^{(1)}$	$\sigma^{(2)}$	d Eq. (23)	D (this work)	D Eq. (22)
0.020	0.010	0.10	0.05	0.95	0.042	0.047
0.010	0.010	0.20	0.10	3.79	0.207	0.184
0.010	0.020	0.10	0.10	1.48	0.309	0.305
0.010	0.020	0.10	0.05	5.27	0.683	0.504
0.005	0.010	0.10	0.05	5.27	0.295	0.252
0.015	0.010	0.10	0.10	−1.44	−0.151	−0.152
0.010	0.010	0.10	0.20	−1.27	−0.273	−0.231
0.020	0.010	0.10	0.10	−2.83	−0.313	−0.305
0.018	0.020	0.05	0.10	−0.98	−0.486	−0.354

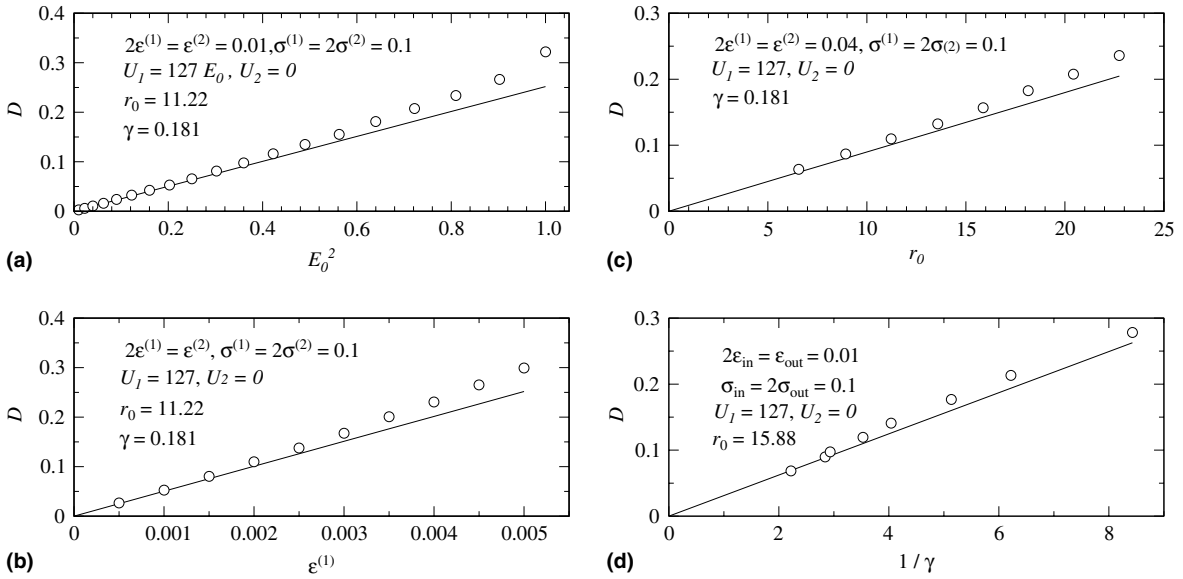

Fig. 3. Variation of drop deformation D with (a) electric field strength E_0, (b) permittivity ϵ, (c) the drop size r_0, and (d) the reciprocal of interfacial tension $1/\gamma$.

3.3. Induced flow field

Another interesting feature is the fluid motion induced by an externally applied electric field. Studies have shown that there are two types of fluid motion, depending on the sign of $(R - S)$ [7,8,39,43], as shown schematically in Fig. 4. If $R < S$, the flow is drawn in from a parallel plane (equator) and expelled along the vertical plane (polar) relative to the electric field; if $R > S$, the flow direction reverses. It is interesting to note that the flow direction is determined only by the relative quantities of R and S, and not related directly to the drop deformation. Obviously, if $R > S$, the discriminating function d is always positive. However, for $R < S$, the drop can deform into a prolate ($d > 0$) or a oblate shape ($d < 0$). Fig. 5(a) shows such relations while Fig. 5(b)–(d) display three typical cases: (b) $R > S$, $d > 0$; (c) $R < S$, $d > 0$; and (d) $R < S$, $d < 0$. Drop deformations are also shown here by the fluid density contours. Clearly, the flow fields from our LBM simulations are in good agreement with the theoretical prediction mentioned above. The flow patterns are also very similar to those from other numerical and experimental studies, both inside and outside the drop [5,7,14].

To study the velocity field more quantitatively, we have also displayed the velocity profiles along the equator and interface in Fig. 6. The symbols are those from our LBM simulations while the solid curves are those from Feng's analysis [39], expressed as follows:

$$\begin{aligned} v_{r,\mathrm{in}} &= U^*[(r/r_0)^3 - (r/r_0)]\cos 2\theta, \\ v_{\theta,\mathrm{in}} &= U^*[(r/r_0) - 2(r/r_0)^3]\sin 2\theta, \\ v_{r,\mathrm{out}} &= U^*[(r_0/r) - (r_0/r)^3]\cos 2\theta, \\ v_{\theta,\mathrm{out}} &= -U^*(r_0/r)^3 \sin 2\theta. \end{aligned} \tag{24}$$

Here v_r and v_θ are, respectively, the radial and tangential velocities in cylindrical coordinates (r, θ) with origin at the drop center; θ was measured counterclockwise from the electric field direction. U^* is called the characteristic velocity representing the maximum velocity at the drop interface as

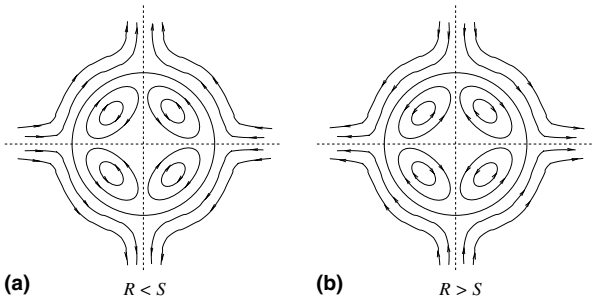

Fig. 4. Schematics of two types of induced flow: (a) $R < S$ and (b) $R > S$. The applied electric field is in the horizontal direction.

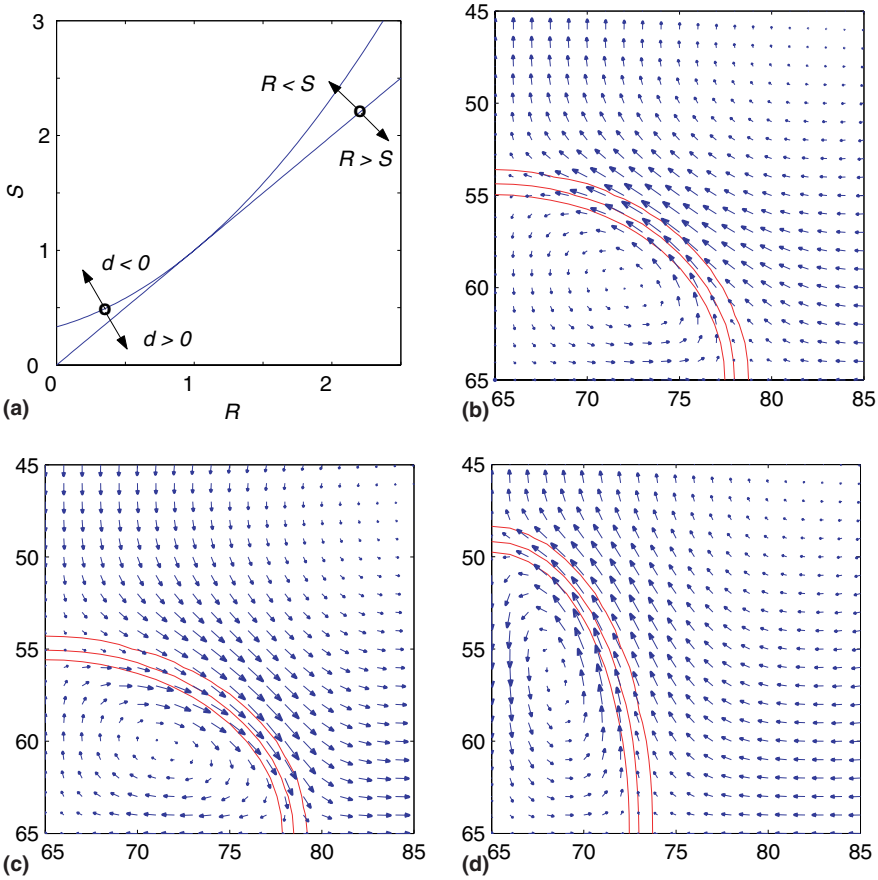

Fig. 5. (a) The relations of drop deformation and induced flow patterns with the dielectric property ratios and three typical cases: (b) $R > S$, $d > 0$; (c) $R < S$, $d > 0$; and (d) $R < S$, $d < 0$. Only a quarter of the central regions are displayed; fluid density contours are also shown to indicate the fluid–fluid interfaces and drop deformations.

$$U^* = \frac{R - S}{2S(1+R)^2} \frac{\epsilon_{\text{in}} E_0^2 r_0}{\mu_{\text{in}} + \mu_{\text{out}}}, \tag{25}$$

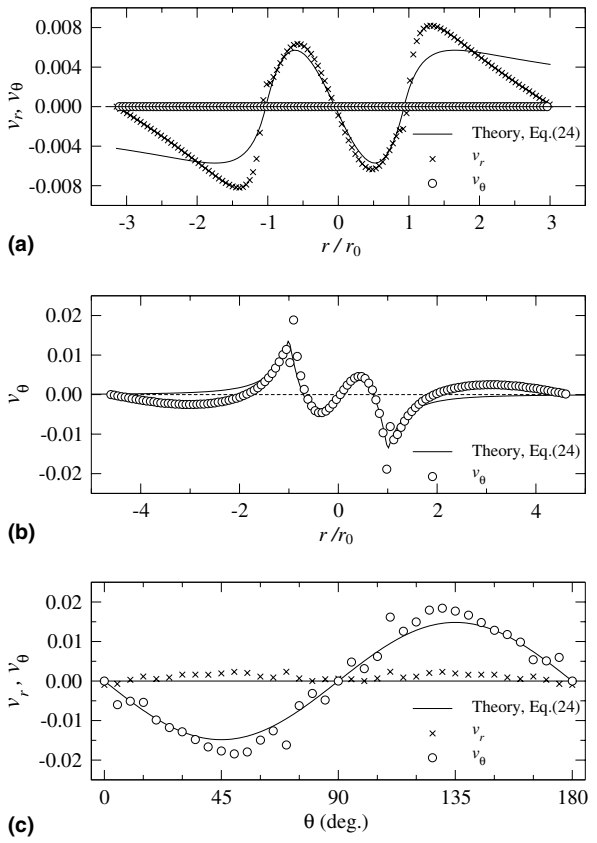

Fig. 6. The velocity profiles from LBM simulations (symbols) compared with theory, Eq. (24) (solid lines): (a) along the equator, (b) in $\theta = 45^\circ$ direction, and (c) along the interface. The crosses (×) and circles (○) denote the radial v_r and tangential v_θ velocity component, respectively. Here $2\epsilon^{(1)} = \epsilon^{(2)} = 0.003, \sigma^{(1)} = 2\sigma^{(2)} = 0.1$, and $r_0 = 19.5$.

and μ is the fluid viscosity. Clearly, the simulated velocities along the drop equator and 45° direction in Figs. 6(a) and (b) agree well with the analytical prediction inside the drop ($-1 \leqslant r/r_0 \leqslant 1$). However, the velocity outside the drop ($|r/r_0| > 1$) deviates from that predicted by the theory. Such a deviation could have resulted from the small simulation domain selected. As a matter of fact, the periodic boundary conditions in our simulation requires the velocity to be zero at the boundary; while that from theoretical prediction will reduce to zero only at an infinite distance. On the other hand, the driven electrical forces concentrate in the interfacial region. Under such boundary and interfacial conditions, the inner fluid region in our LBM simulations actually is very similar to that of the theoretical model in Ref. [39]; however, the outer regions in these two cases were quite different: one finite and one infinite. Hence, it is reasonable to see in Figs. 6(a) and (b) that the simulated and theoretical velocity profiles inside the drop agree much better than those outside.

In Fig. 6(b), we noticed a tangential velocity jump across the fluid interface ($r/r_0 = \pm 1$). This phenomenon has also been observed by Ginzbourg using a lattice gas method [44]. In another study, Chin et al. [37] simulated a Poiseuille flow for a layer of Fluid 1 which is sandwiched between two layers of Fluid 2 in a 2D channel using also the Shan–Chen model. Their LBM and analytical velocity profiles were found to be in good agreement, except a small deviation (in velocity jump) near the interfacial regions. This phenomenon was not addressed and discussed in [37]. Report of such a phenomenon is also rare in literature and could

deserve a more systematic study. The reason for this velocity jump is unclear and could result from the direct use of the Shan–Chen model or LBM in treating interfacial regions. Nevertheless, the deviation in Fig. 6(b) occurs only in the relatively small interfacial region and appears to have no impact on our results. Moreover, the comparison and analysis shown in Fig. 6 were not available in other numerical EHD studies [42,14], Since the interface from a multiphase/multicomponent LBM is a diffuse region instead of a sharp surface and, in order to study the velocity along the interface, we have assumed the *interface* to consist of an iso-density contour where the least amount of mass transfer occurs [cf. Fig. 5(b)−(d)]. The velocity along such an *interface* is displayed in Fig. 6(c) and was obtained by interpolation using the nearest neighbors. In principle, the velocity profiles agree with the theoretical analysis: the radial component v_r is about zero; and the tangential component v_θ follows the $\sim\sin 2\theta$ trend. The scatters could be caused by our interpolation procedures and the uncertainty of the *interface* position as v_r and v_θ deviate from the theoretical prediction in a similar fashion. The above comparison and discussion with respect to the drop deformation and fluid velocity demonstrate the validity of our LBM scheme in electrohydrodynamics studies.

4. Summary

We have implemented the lattice Boltzmann method to study electrohydrodynamics. An algorithm is presented by incorporating electric field effects to the fluid motions. Simulations were performed to investigate deformation of a 2D drop being suspended in another fluid as a result of electric field, conductivity, permittivity and interfacial tension effects. The deformation and flow behaviors from our simulations are in good agreement with other studies. Given that no special treatment of fluid–fluid interfaces is required in multiphase/ multicomponent LBM, our scheme could be an excellent alternative to electrohydrodynamics studies than traditional computational fluid dynamics methods. The algorithm and simulation presented in this study can also be easily extended to the more complex systems. To our knowledge, this represents the first LBM study on multiphase electrohydrodynamics.

Acknowledgments

The authors thank Prof. Stéphane Zaleski and the unknown Referees for valuable suggestions and comments. This work was supported, in part, by the Canada Research Chair (CRC) Program and Natural Sciences and Engineering Research Council of Canada (NSERC). J.Z. acknowledges the financial support from the Alberta Ingenuity through a studentship fund.

References

[1] D.A. Saville, Annu. Rev. Fluid Mech. 29 (1997) 27.
[2] J.R. Melcher, G.I. Taylor, Annu. Rev. Fluid Mech. 1 (1969) 111.
[3] G. Taylor, Proc. R. Soc. Lond. A 313 (1969) 453.
[4] A. Castellanos, A. Gonzalez, IEEE Trans. Dielectr. Electr. Insul. 5 (3) (1998) 334.
[5] J.-W. Ha, S.-M. Yang, Phys. Fluids 12 (4) (2000) 764.
[6] R.S. Allan, S.G. Mason, Proc. R. Soc. Lond. A 267 (1962) 45.
[7] G. Taylor, Proc. R. Soc. Lond. A 291 (1966) 159.
[8] S. Torza, R.G. Cox, S.G. Mason, Philos. Trans. R. Soc. Lond. 269 (1971) 259.
[9] P.A. Arp, R.T. Roister, S.G. Mason, Adv. Colloid Interface Sci. 12 (1980) 295.
[10] O. Vizika, D.A. Saville, J. Fluid Mech. 239 (1992) 1.
[11] D.A. Saville, Phys. Rev. Lett. 71 (1993) 2907.
[12] M. Trau, S. Sankaran, D.A. Saville, I.A. Aksay, Nature 374 (1995) 437.

[13] M. Trau, S. Sankaran, D.A. Saville, I.A. Aksay, Langmuir 11 (1995) 4665.
[14] J.Q. Feng, Proc. R. Soc. Lond. A 455 (1999) 2245.
[15] J.-W. Ha, S.-M. Yang, Phys. Fluids 12 (7) (2000) 1671.
[16] S.M. Lee, D.J. Im, I.S. Kang, Phys. Fluids 12 (8) (2000) 1899.
[17] P.K. Notz, O.A. Basaran, J. Colloid Interface Sci. 213 (1999) 218.
[18] S. Chen, G.D. Doolen, Annu. Rev. Fluid Mech. 30 (1998) 329.
[19] S. Succi, The Lattice Boltzmann Equation, Oxford University Press, Oxford, 2001.
[20] X. Shan, H. Chen, Phys. Rev. E 47 (3) (1993) 1815.
[21] M.R. Swift, W.R. Osborn, J.M. Yeomans, Phys. Rev. Lett. 75 (5) (1995) 830.
[22] J. Zhang, B. Li, D.Y. Kwok, Phys. Rev. E 69 (2004) 032602.
[23] N.S. Martys, H. Chen, Phys. Rev. E 53 (1996) 743.
[24] S. Hou, X. Shan, Q. Zou, G.D. Doolen, W.E. Soll, J. Comput. Phys. 138 (1997) 695.
[25] B.R. Sehgal, R.R. Nourgaliev, T.N. Dinh, Prog. Nucl. Energy 34 (1999) 471.
[26] L. Fan, H. Fang, Z. Lin, Phys. Rev. E 63 (2001) 051603.
[27] Q. Kang, D. Zhang, S. Chen, Phys. Fluids 14 (9) (2002) 3203.
[28] A. Frohn, N. Roth, Dynamics of Droplets, Springer, Berlin, 2000.
[29] H. Chen, S. Chen, W.H. Matthaeus, Phys. Rev. A 45 (1992) R5339.
[30] Y.H. Qian, D. d'Humieres, P. Lallemand, Europhys. Lett. 17 (1992) 479.
[31] X. Shan, G.D. Doolen, J. Stat. Phys. 49 (1995) 2941.
[32] X. Shan, G.D. Doolen, Phys. Rev. E 54 (1996) 3614.
[33] D. Landau, E. Lifshitz, Electrodynamics of Continuous Media, Pergamon Press, New York, 1960.
[34] J.S. Rowlinson, F.L. Swinton, Liquids and Liquid Mixtures, third ed., Butterworth Scientific, London, 1982.
[35] X. He, N. Li, Comput. Phys. Commum. 129 (2000) 158.
[36] S. Melchionna, S. Succi, Phys. Fluids 120 (9) (2004) 4492.
[37] J. Chin, E.S. Boek, P.V. Coveney, Philos. Trans. R. Soc. Lond. A 360 (2002) 547.
[38] Z.L. Yang, T.N. Dinh, R.R. Nougaliev, B.R. Sehgal, Int. J. Heat Mass Transfer 44 (2001) 195.
[39] J.Q. Feng, J. Colloid Interface Sci. 246 (2002) 112.
[40] P.H. Rhodes, R.S. Snyder, G.O. Roberts, J. Colloid Interface Sci. 129 (1) (1989) 78.
[41] J.-W. Ha, S.-M. Yang, J. Fluid Mech. 405 (2000) 131.
[42] J.Q. Feng, T. Scott, J. Fluid Mech. 311 (1996) 289.
[43] J.C. Baygents, N.J. Rivette, H.A. Stone, J. Fluid Mech. 368 (1998) 359.
[44] I. Ginzbourg, Boundary condition problems in lattice gas methods for single and multiple phases, Ph.D. thesis, University of Paris VI, 1994.